

Viscous flow of a volatile liquid on an inclined
heated surface

Vladimir S. Ajaev

Department of Mathematics,
Southern Methodist University

Dallas, TX 75275

May 30, 2004

Running title: VISCOUS FLOW ON HEATED SURFACE

Corresponding author:

Vladimir S. Ajaev

tel.(214)768-3629

fax:(214)768-2355

E-mail: ajaev@mail.smu.edu

Abstract

We investigate the effects of evaporation on a gravity driven flow of a viscous liquid on a heated solid. Vapor molecules are adsorbed on the dry areas of the solid and form a microscopic adsorbed film. The thickness of this film is calculated from the formulas for disjoining pressure and the principles of equilibrium thermodynamics. A lubrication-type approach is used to derive an evolution equation capable of describing both the macroscopic shape of the vapor-liquid interface and the adsorbed film on the vapor-solid interface. Under the conditions of negligible evaporation, the numerical solution of the evolution equation predicts translational motion and formation of capillary ridge, in agreement with previous investigations. Moderate evaporation is shown to slow down the flow and decrease the height of the capillary ridge, which implies stabilizing effect of evaporation on the well-known instability observed in gravity driven thin film flows. We also study combined effects of evaporation and thermocapillary stresses and show that the latter act to reduce the velocity of the downward motion, but increase the height of the capillary ridge. Apparent contact angles are found from the solution and shown to increase with evaporation and contact line speed. For strong evaporation, steady state solutions are found such that evaporation balances the downward motion of the interface under the action of gravity.

Key words: viscous flows, evaporation, contact lines, disjoining pressure, thermocapillarity

1 Introduction

Flows in thin films of viscous liquids under the action of body forces are important for a number of industrial applications that involve coating of a solid surface with a thin layer of another material. Examples include manufacture of photographic film and magnetic storage disks. Applications of similar flows in microfluidics have been also discussed in recent studies of spreading on chemically patterned surfaces [1] and optical control methods for microscale flows [2].

Mathematical models of viscous flows driven by body forces usually rely on the assumption that evaporation from the liquid surface is negligible even though in experiments liquids often spread on heated solid substrates [2, 3]. Heating is introduced in experiments in order to control the flow [2, 4] or is present in the system due to the nature of the applications considered, e.g. in thin-film flows over hot surfaces during unsteady start-up and shut-down operation of a micro heat pipe [5]. In the latter application evaporation clearly cannot be neglected since heat pipes involve volatile liquids at relatively high temperatures.

The goal of the present work is to investigate the effect of evaporation on gravity-driven viscous flows in the framework of a lubrication-type approach which relies on the assumption of liquid film thickness being small compared to all other macroscopic length scales in the problem. This approach has been used for a variety of gravity-driven flows over solid surfaces [6, 7]; its validity has been discussed by Goodwin & Homsy [8] and Mazouchi et al. [9]. Evaporation can be easily incorporated into the interfacial boundary conditions [10], but its effect on the local conditions at the moving contact line, i.e. the region where the surface of the liquid film comes into contact with the solid, requires a more

detailed discussion.

We introduce a model of moving contact lines in the presence of phase change based on the ideas from earlier work on steady menisci in contact with heated surfaces by Potash and Wayner[11] and Moosman and Homsy[12]. It relies on the description of dry areas by microscopic adsorbed films which are in thermodynamic equilibrium with both solid and vapor phases. Such equilibrium can be achieved for non-zero film thickness due to action of London-van-der-Waals forces. Macroscopic shape of the vapor-liquid interface has to match the adsorbed-film solution asymptotically. The contact line is then described as the region of rapid change of interfacial curvature where such matching takes place. The approach has been used successfully for finding local steady-state solutions near contact lines on heated surfaces [13, 14]. A similar approach has been used by Lyushnin et al. [15] in their studies of dewetting in thin films of polar liquids.

Most mathematical models of contact lines on heated surfaces [11, 12] rely on the assumption that the liquid is perfectly wetting under the isothermal conditions, which is not the case for typical coating flows. The effect of evaporation on dynamic contact angles for partially wetting volatile liquids has been discussed by Anderson and Davis [16] in the framework of a macroscopic model. However, the relationship between the microscopic details of the contact line region, as described by disjoining pressure curves, and the macroscopic solution for the liquid flow, is still not completely understood. We attempt to resolve the issue by incorporating carefully derived formulas for disjoining pressure [17, 18, 19, 20] into our model of liquid flow. These formulas take into account the dependence of the disjoining pressure not only on film thickness, but also on the slope and

the curvature of the interface.

Local analysis of the contact line region is clearly not sufficient for describing gravity-driven flows over solid surfaces since contact line motion in such flows is coupled to the global shape of the vapor-liquid interface. The challenges in describing such coupling have been addressed in the context of both steady and oscillating constrained vapor bubbles [21, 22]. Bubble shapes have been found such that the position of the contact line is not prescribed but rather determined as part of the solution. In the present work we use the same global approach to develop a model for viscous flow of a volatile liquid, either perfectly or partially wetting, on an inclined heated surface. We investigate the effect of evaporation on the evolution of the vapor-liquid interface. Implications of the results to stability criteria of the interface are also discussed. We do not attempt to carry out numerical simulations of the rivulet instability [23] in the presence of evaporation, although our approach can be used for such simulations as well.

The paper is organized as follows. Nondimensional governing equations and boundary conditions are formulated in Section 2. In section 3, we describe the lubrication-type approach which allows us to reduce the original system of governing equations and boundary conditions to an evolution equation for liquid film thickness. Details of the numerical solution of this differential equation are presented. Models of the disjoining pressure are also discussed. In Section 4 we discuss evolution of the interface for different material properties and heating conditions and study apparent contact angles as functions of nondimensional parameters. Finally, the key findings are summarized in Section 5.

2 Formulation

We consider flow of a volatile viscous liquid of density ρ and viscosity μ on a heated solid surface, as shown in Fig. 1a. The solid surface is at an angle α to the horizontal direction. The nondimensional temperature profile along the surface, shown in Fig 1b, simulates a finite-size heater; temperature is scaled by the equilibrium saturation temperature, T_S^* . The main physical effects of heating on the gravity driven flow are the mass loss at the vapor-liquid interface due to evaporation and the thermocapillary stress. The latter is acting along the interface which can no longer be considered isothermal in the presence of heating.

The solution far away from the leading edge of the advancing vapor-liquid interface is assumed to be a parallel viscous flow in a film of uniform thickness b , which is used as the scale for all length variables in this section. The governing equations for nondimensional liquid velocity \mathbf{v} , pressure p , and temperature T are written in the form

$$-\frac{1}{C}\nabla p + \nabla^2 \mathbf{v} + \mathbf{e}_g = 0, \quad (1)$$

$$\nabla \cdot \mathbf{v} = 0, \quad (2)$$

$$\nabla^2 T = 0. \quad (3)$$

Here \mathbf{e}_g is the unit vector in the direction of gravity. We use the capillary scale, σ_0/b , for the pressure, where σ_0 is the surface tension at the temperature T_S^* . The velocity scale U is the characteristic velocity of the parallel gravity-driven flow away from the contact line [9],

$$U = \frac{\rho g b^2}{\mu}, \quad (4)$$

where g is the acceleration of gravity; time is scaled with b/U . We introduce the capillary number according to

$$C = \frac{\mu U}{\sigma_0}.$$

Both inertia effects and convective heat transfer are assumed negligible. The fluid flow in the vapor phase directly above the liquid is in general coupled to the flow in the liquid. However, in this study we use the one-sided model of evaporation [10]. It implies that the density, dynamic viscosity, and thermal conductivity of the vapor phase are very small compared to those of the liquid. Therefore, we take the limit when the corresponding nondimensional ratios approach zero. However, the vapor density is retained in the boundary conditions where it multiplies the vapor velocity, which can be large.

Let us define the evaporation number according to

$$E = \frac{kT_S^*}{\rho U \mathcal{L} b},$$

where k is the thermal conductivity of the liquid, \mathcal{L} is the latent heat of vaporization; the characteristic velocity U is defined by equation (4) above. The evaporation number is the ratio of the timescale of the downward gravity driven motion of the liquid to the evaporative timescale. We note that the definition of the evaporation number in the present work is different from that in Burelbach et al. [10] where a viscous velocity scale, $\mu/\rho b$, is used instead of Eqn. (4).

The nondimensional conditions of conservation of mass and energy at the liquid surface are

$$EJ = (\mathbf{v} - \mathbf{v}^I) \cdot \mathbf{n}, \quad (5)$$

$$J = -\mathbf{n} \cdot \nabla T. \quad (6)$$

Here \mathbf{n} is the unit normal vector to the interface pointing into the liquid, \mathbf{v}^I is the velocity of the interface, and the scaled mass flux at the vapor-liquid interface is defined as

$$J = J^* \mathcal{L} b / k T_S^*,$$

where J^* is the dimensional mass flux. The normal and shear stress balances at the interface are written in the form

$$\mathbf{n} \cdot \mathbf{T} \cdot \mathbf{n} = \nabla \cdot \mathbf{n} + \Pi_0 - p_v, \quad (7)$$

$$\mathbf{t} \cdot \mathbf{T} \cdot \mathbf{n} = -M \mathbf{t} \cdot \nabla T. \quad (8)$$

Here p_v is the scaled vapor pressure, and the condition (8) is satisfied for any tangent vector \mathbf{t} . The nondimensional stress tensor, \mathbf{T} , and disjoining pressure, Π_0 , are the ratios of corresponding dimensional quantities to the capillary pressure scale, σ_0/b . The disjoining pressure is assumed to be due to van der Waals forces only; it can be expressed in terms of the interface shape as described in Wu & Wong [20]. We also assume that the surface tension is a linear function of temperature,

$$\sigma = \sigma_0 - \gamma(T^* - T_S^*),$$

and introduce the modified Marangoni number $M = \gamma T_S^* / \sigma_0$. The interfacial temperature T^i is related to the local mass flux and pressure jump at the interface through the non-equilibrium condition [21] written in the form:

$$K J = \delta(p - p_v) + T^i - 1, \quad (9)$$

where

$$K = \frac{k T_S^*}{2 \rho_v \mathcal{L}^2 b} \sqrt{2 \pi \bar{R} T_S^*}, \quad \delta = \frac{\sigma_0}{\mathcal{L} \rho b}.$$

Here \bar{R} is the gas constant per unit mass, ρ_v is the vapor density. The kinetic parameter, K , measures the relative importance of kinetic effects at the interface. The parameter δ characterizes the effect of changes in liquid pressure on the local phase-change temperature at the interface. Both parameters are typically rather small.

At the solid-liquid interface the liquid velocity is zero and the nondimensional value of temperature, T_0 , is prescribed as illustrated in Fig. 1b. Initial condition for film thickness in the numerical simulations below is chosen in the form of a step-function.

3 Lubrication-type analysis

In this section we consider the limit of small capillary numbers. In order to obtain physically meaningful solutions we consider distinguished limits when physical quantities, as well as parameters of the problem, scale as certain powers of the capillary number.

Let us assume that the nondimensional Cartesian coordinates (x, y) shown in Fig. 1a are such that y is scaled by b and x is scaled by $b/C^{1/3}$. These scales are commonly used to account for the fact that the length scale in the x -direction is much larger than the film thickness. In order to derive lubrication-type equations in which viscous stresses balance capillary pressure gradients, the temperature, pressure, and velocity component in the vertical direction, v , are rescaled according to

$$(T - 1, p, v) = C^{2/3}(\bar{T}, \bar{p}, \bar{v}).$$

The governing equations at the leading order then take the following form:

$$-\bar{p}_x + u_{yy} + \sin \alpha = 0, \quad (10)$$

$$-\bar{p}_y = 0, \quad (11)$$

$$u_x + \bar{v}_y = 0, \quad (12)$$

$$\bar{T}_{yy} = 0. \quad (13)$$

Let us now formulate the re-scaled boundary conditions at the liquid-vapor interface which is described by its nondimensional thickness h . In order to include the vapor mass flux into the leading-order mass-conservation condition one has to rescale the flux according to

$$J = C^{2/3} \bar{J}, \quad \bar{J} = O(1).$$

With this choice and the above length and velocity scales, equation (5) becomes

$$\bar{E} \bar{J} + u h_x - \bar{v} = h_{\bar{t}}. \quad (14)$$

Here we also rescale time and the evaporation number according to

$$(t, E) = C^{-1/3} (\bar{t}, \bar{E}).$$

We note that the value of E can be large for microscale flows, which justifies the above scaling. The case of small E , which is also relevant for many gravity driven viscous flows, is recovered later by taking the limit of $\bar{E} \rightarrow 0$.

The re-scaled version of (6), condition for conservation of energy, at leading order is given by

$$\bar{J} = -\bar{T}_y. \quad (15)$$

Most of the terms in the normal and shear stress balances, equations (7) and (8), drop out of the leading order in C , so the interfacial stress conditions take a relatively simple form,

$$\bar{p} - \bar{p}_v = -h_{xx} - \Pi \quad (16)$$

$$u_y = -M(\bar{T}_x + h_x \bar{T}_y). \quad (17)$$

The re-scaled disjoining pressure $\Pi = \Pi_0 C^{-2/3}$ is usually assumed to be inversely proportional to the cube of the film thickness. However, it has been also argued that Π has to be a function of derivatives of the thickness [18, 20]. In the present work, we adopt the general formula for the disjoining pressure derived by Wu & Wong [20], which is applicable to both perfectly and partially wetting liquids. In our formulation it can be written as

$$\Pi = \frac{\varepsilon}{h^3} \left[1 + \beta(2hh_x^2 h_{xx} - h_x^4) \right], \quad (18)$$

where the nondimensional constants ε and β are functions of the material properties and the capillary number. However, since equation (18) is still lacking experimental verification, we ran several simulations for the standard dependence of the disjoining pressure on the film thickness to verify that the main qualitative conclusions of the paper are still valid for $\beta = 0$.

We write the non-equilibrium condition at the interface as

$$K\bar{J} = -\delta(h_{xx} + \Pi) + \bar{T}^i. \quad (19)$$

The right-hand side of equation (19) represents contributions to mass flux due to changes in interfacial curvature, disjoining pressure, and local temperature of the heated solid surface. The conditions for velocity components and temperature at the solid boundary are the same as in the previous section.

Let us now solve the re-scaled system of governing equations and boundary conditions. First, let us note that the mass flux \bar{J} is related to the interfacial temperature according to the non-equilibrium condition at the interface, equation (19). The interfacial temperature, \bar{T}^i , can be expressed in terms of the known temperature of the solid surface since according to the scaled heat-conduction equation the temperature profile in the film is linear in y . Therefore, the flux \bar{J} can be expressed in terms of the scaled difference between the wall and the saturation temperatures, \bar{T}_0 , in the following form:

$$\bar{J} = \frac{\bar{T}_0 - \bar{\delta}(h_{xx} + \Pi)}{K + h}. \quad (20)$$

The momentum equation (10) can be integrated twice to give the lubrication-type velocity profile

$$u = \frac{1}{2}(\bar{p}_x - \sin \alpha)(y^2 - 2yh) - M\bar{T}_x^i y. \quad (21)$$

We now substitute this velocity profile into the mass-conservation condition at the interface to obtain

$$h_{\bar{t}} + \bar{E}\bar{J} = \frac{1}{3}(h^3\bar{p}_x)_x + \frac{M}{2}[h^2(\bar{T}_0 - \bar{J}h)_x]_x. \quad (22)$$

The expression for liquid pressure from the normal-stress balance, eqn. (16), can be substituted into equation (22) to obtain the following differential equation for the film thickness $h(x, \bar{t})$:

$$h_{\bar{t}} + \bar{E}\bar{J} + \frac{1}{3}[h^3(h_{xx} + \Pi)_x]_x + \sin \alpha h^2 h_x - \frac{M}{2} [h^2(\bar{T}_0 - \bar{J}h)_x]_x = 0. \quad (23)$$

Here the flux \bar{J} is expressed in terms of \bar{T}_0 and h according to eqn. (20) and the disjoining pressure Π is assumed to be in the form given by eqn. (18). Equation

(23) relates the rate of change of thickness to the evaporative mass loss (the second term on the right-hand side) and the viscous flow rate. The latter has components due to capillary and disjoining pressure gradients, gravity, and thermocapillary stress.

Let us now discuss boundary conditions for equation (23). The origin of the coordinate system sketched in Fig. 1a corresponds to the region of uniform film thickness and parallel gravity-driven flow. Let us denote the length of the computational domain by L and assume that near $x = L$ the solid surface is macroscopically dry, which in our formulation implies that the height of the interface, $h(x, \bar{t})$, is equal to the thickness of the microscopic adsorbed film. In this region the evaporative mass flux is suppressed by London-van-der-Waals forces. Thickness of the equilibrium adsorbed film is found from the condition of zero mass flux in equation (20):

$$h_{af} = \left(\frac{\delta\varepsilon}{\bar{T}_H} \right)^{1/3}. \quad (24)$$

We note that a microscopic film on a macroscopically dry solid surface, often referred to as the precursor film, was discussed in several studies of coating flows [6, 7, 24], but its thickness was introduced as a parameter of the model. Golovin et al. [25] investigated precursor films of non-uniform thickness by using the balance between van der Waals forces and convective transport, but did not consider the effects of evaporation. In the present work, the thickness of the microscopic film is determined based on the principles of equilibrium thermodynamics as a function of heating conditions and material properties of the liquid according to equation (24).

Since the adsorbed film is flat, all derivatives of h have to be zero at $x = L$.

This condition was relatively easy to satisfy for steady state [14] when an ordinary differential equation was solved using a shooting method. However, for unsteady contact line it is not clear *a priori* why the value of L exists such that the film is indeed flat there. A remarkable feature of the numerical solution illustrated below is that only two boundary conditions are sufficient to ensure that the film is flat at $x = L$. We choose these conditions in the form:

$$h(L) = h_{af}, \quad h_x(L) = 0.$$

At the point $x = 0$ which corresponds to incoming parallel flow, we impose two conditions,

$$h(0) = 1, \quad h_{xxx}(0) = 0.$$

Departures from the parallel flow near $x = 0$ are verified to be negligible for sufficiently large L after the solution is obtained.

Let us now specify the temperature profile $\bar{T}_0(x)$ in equation (23). In order to simulate a finite-size heater and preserve the parallel-flow structure of the solution near $x = 0$ it is convenient to choose the profile in the form

$$\bar{T}_0(x) = \bar{T}_H \left(\frac{1}{2} + \frac{1}{\pi} \tan^{-1} \frac{x - x_0}{l} \right). \quad (25)$$

Here the length scale l is typically much smaller than L . In the simulations below we assume $l = 0.2$, $x_0 = 0.2L$, unless noted otherwise.

Equation (23) with the above boundary conditions is solved numerically using finite-difference approach [26] with a number of mesh points varying between 400 and 1000 to verify convergence. Standard DVODE solver [27] is used to describe evolution in time numerically. We start each simulation with an artificial profile which is a step function that jumps from 1 to a value slightly above h_{af} at the

point $x = L/3$ and run it for the period of time $\Delta t = 1$. The result is then used as the initial condition at $\bar{t} = 0$. We note that with this choice of initial conditions the dry area described by the adsorbed film always remains in the heated part of the solid surface where the nondimensional temperature is close to \bar{T}_H .

4 Results and discussion

4.1 Weak evaporation limit

Several mathematical models have been developed to describe gravity driven flows of liquids on solid surfaces under the conditions of negligible evaporation [6, 7, 8, 24]. Let us try to recover some of the results of the previous investigations by solving Eqn. (23) in the regime when the effect of evaporation on the flow is small, which in our formulation implies that the scaled evaporation number, \bar{E} , is small. We assume that $\bar{E} = 10^{-4}$ and choose the following representative values of the other nondimensional parameters: $K = 0.2, \delta = 10^{-3}, \varepsilon = 10^{-6}, \bar{T}_H = 0.5$. Numerical solution of equation (23) with the initial and boundary conditions described in the previous section indicates that after a short period of transient evolution a regime is attained such that the interface motion is described as a translation in the x -direction with negligibly small variations of its shape. A typical interface shape in this regime is shown in Fig. 2a. This type of evolution, as well as the interface shape showing a capillary ridge, are very similar to the well-known results of the previous investigations [8, 9]. A detailed comparison shows that the height of the capillary ridge is typically less than the corresponding value under similar conditions in [8], which is likely due to the limitations of

the lubrication-type approach used in the present work. Good agreement with previous work can be demonstrated only for the values of \bar{E} below 10^{-4} , which provides a simple nondimensional criterion for the weak evaporation limit. This is especially important since mathematical models of nonisothermal thin-film flows in microfluidic devices often rely on the assumption of negligible evaporation without specifying quantitative criteria for validity of this assumption.

Macroscopic interface shapes in gravity driven thin film flows are typically not very sensitive to the details of the contact line model, as was shown by comparison of Navier-type slip models and precursor film models [28]. Our results also support this conclusion. The macroscopic interface shapes for weak evaporation in the present work are essentially the same as in [8] even though our description of the contact line region is different. In fact, the interface in our solution never comes into contact with the solid surface; instead it approaches a microscopic adsorbed film. This is clearly seen in Fig. 2b which shows the transition between the macroscopic film and the adsorbed film in a linear-logarithmic plot. (We note that the adsorbed film in Fig. 2b is indeed always flat near $x = L$, i.e. *all* derivatives of h are zero there, even though only the condition for the first derivative is enforced by the numerical algorithm). Thus, what appears to be a contact line in Fig. 2a, is in fact a localized region of very high curvature moving from the left to the right. We still often refer to it as contact line based on the macroscopic picture of the solution.

We note that even for \bar{E} below 10^{-4} , the effects of evaporation are not completely eliminated, but rather localized in the transition region between the macroscopic interface and the adsorbed film. In order to observe the effects

of evaporation on larger macroscopic length scales, one has to make evaporative contributions in equation (23) stronger, e.g. by increasing the value of the evaporation number. This is discussed in the next subsection.

4.2 Effects of evaporation

Let us increase the scaled evaporation number while keeping all other parameters fixed ($K = 0.2, \delta = 10^{-3}, \varepsilon = 10^{-6}, \bar{T}_H = 0.5, M = 0, \beta = 1, \alpha = \pi/4$). Changes in shape and dynamics are very small as long as the scaled evaporation number is below 10^{-3} . In the range of values of \bar{E} between 10^{-3} and 0.03, interface behavior can still be described qualitatively as slow gravity-driven thin-film flow down the slope, but the velocity of downward motion and the interface shapes now depend on evaporation. Let us define V as the velocity of the point of the maximum height of the interface at $\bar{t} = 100$. A large value of \bar{t} is chosen here to make sure that transients due to somewhat artificial initial condition have decayed. The value of V as a function of \bar{E} is shown in Fig. 3. Evaporation clearly slows down the interface significantly even for relatively small values of \bar{E} . Physical explanation of this result can be given based on the global mass balance in the system. The incoming flow supplies a fixed amount of liquid per unit time, while the mass loss due to evaporation becomes higher as \bar{E} is increased. If one assumes that evaporation is localized near the leading edge of the interface, the mass loss due to evaporation can be expressed as a linear function of \bar{E} and therefore the velocity is also expected to vary linearly with the evaporation number. Small departures from the linear behavior seen in Fig. 3 are due to evaporation in the regions away from the leading edge. This contribution to the total evaporative

mass flux also results in small variations of interface shape over long periods of time. Thus, interface motion down the slope can no longer be described as simple translation in the x -direction if evaporation is present.

In order to illustrate evolution of interface shapes let us plot the maximum height of the capillary ridge, h_{max} , as a function of time. Results for two different values of the evaporation number are shown in Fig. 4a, where the weak evaporation data is also shown by dot-dashed lines for comparison. After an initial transient period, h_{max} slowly decays. The height of the capillary ridge tends to be smaller for stronger evaporation. It is generally accepted that h_{max} is important for stability (except for relatively high capillary numbers when no ridge is formed [29]), with larger values of the height corresponding to more unstable flows [8]. Therefore, our results imply that evaporation can have a stabilizing effect on gravity driven flow at low capillary numbers.

Evaporation number is an important parameter which characterizes the material properties of liquids used in experiments. It is larger for liquids which are more volatile. An estimate of the evaporation number gives an important criterion for significance of evaporation under given experimental conditions. However, \bar{E} may be difficult to vary in experiments. Therefore, we also present the results in terms of \bar{T}_H , the scaled heater temperature. This is a natural control parameter in experiments since it can be easily varied over a wide range by changing the heating conditions. Results for the maximum interfacial height versus time for different nondimensional heater temperatures and fixed $\bar{E} = 10^{-3}$ are shown in Fig. 4b. Higher temperature of the heater results in slower motion and lower height of the capillary ridge. The height of the capillary ridge can be controlled

easily by changing the heater temperature.

Let us now investigate how interface evolution depends on the strength of the thermocapillary forces, measured by the modified Marangoni number M . In the computations above the attention was focused on the effects of evaporation, so the value of M was assumed to be zero. Figure 5 shows typical evolution of the position of the interface maximum and the height of the capillary ridge for two different values of M . Clearly, thermocapillary forces tend to slow the downward motion. However, the height of the capillary ridge is increased due to thermocapillary flow. This can be explained by noting that thermocapillary stress acts in the direction from the hotter regions near the contact line towards the colder regions away from it, so more liquid tends to accumulate in the capillary ridge. We note that the solution is not very sensitive to the value of β , as can be seen from comparison between Fig. 5b for $M = 0$, computed at $\beta = 0$, and the corresponding data for $\beta = 1$ in Fig. 4.

Finally, let us increase the evaporation number above the maximum value of 0.01 used in Figures 4 and 5. In this regime the evaporation can be strong enough to compensate the gravity-driven downward motion of the interface. This is clear from Fig. 6, where the position of the interfacial maximum is plotted as a function of time for three different values of \bar{E} . The plot indicates that a steady state is attained for $\bar{E} = 0.04$ (solid line).

4.3 Apparent contact angles

Mathematical model developed in the present work does not require a contact angle to be prescribed. The interface shape is obtained by solving equation (23)

with appropriate boundary conditions in the adsorbed film rather than contact-angle conditions. The notion of the contact angle, however, can still be useful for the purposes of characterization of interface shapes and comparison with previous experimental and theoretical studies. Therefore we introduce an *apparent* contact angle defined as the maximum slope of the interface in the region where transition to the adsorbed film occurs.

Results for the apparent contact angle, recorded at $\bar{t} = 10$, versus heater temperature are shown in Fig. 7a. We note that the dependence is nonlinear as a result of global coupling between the effects of heating and liquid flow on the apparent contact angle. For stronger heating, the velocity of downward motion is reduced, as required by mass balance discussed in the previous subsection. Thus, the dynamic contribution to the value of the apparent contact angle is reduced and the actual value of the contact angle is less than one may expect based on linear models.

In order to better understand the dynamic contribution to the apparent contact angle we changed the value of the inclination angle under fixed heating conditions ($\bar{T}_H = 1$) and recorded the values of the contact angle in Fig. 7b. Since the velocity of the incoming flow and thus the velocity of downward motion of the interface depends on $\sin \alpha$, the apparent contact angle is recorded as a function of $\sin \alpha$. The contact angle increases monotonically, but the rate of increase is less for higher $\sin \alpha$.

The local structure of the flow near contact lines is typically similar for different global shapes of vapor-liquid interfaces, so the properties of the contact angles can also be expected to show similarity. The results for apparent contact

angles shown in Fig. 7 are in qualitative agreement with many related experimental studies of contact lines with evaporation [30, 31]. However, we do not attempt quantitative comparisons since no measurement of contact angles for gravity driven flows of volatile liquids on inclined heated surfaces has been reported in the literature.

5 Conclusions

We have developed a mathematical model for viscous flow of a volatile liquid on an inclined heated surface using a lubrication-type approach. Evolution equation for interface position is derived and solved numerically with boundary conditions which account for the microscopic adsorbed film on the dry area of the solid. Moving contact line is defined from the numerical solution as a localized region of high interfacial curvature. Since the adsorbed film is very thin, the interface comes within few molecular layers from the solid, which justifies our use of the term contact line. Apparent contact angles are found by recording the maximum slope of the interface. They are shown to depend on contact line speed, heating conditions and material properties of the liquid. The apparent contact angle increases with heater temperature and with contact line speed, consistent with related experimental observations. We note that our approach to modeling moving contact lines through disjoining pressure extends the earlier work of Potash and Wayner [11] and Moosman and Homsy [12] to unsteady case and to partially wetting liquids.

We identify the conditions when evaporation is weak and show that the present

approach allows us to recover the results of previous investigations in the limit of negligible evaporation. It confirms that the macroscopic interface shapes are not very sensitive to the details of the contact line model since previous studies used either slip models or precursor film models which are different from the treatment of the contact line region in the present work.

We show that even moderate evaporation can have a significant effect on interface shapes. Evaporation slows down the gravity-driven flow down the inclined surface and decreases the height of the capillary ridge, which implies that it can have a stabilizing effect on the rivulet instability at low capillary numbers. Thermocapillary effect is shown to slow down the interface and increase the height of the capillary ridge. We also show that evaporation can be strong enough to balance the downward gravity driven flow in such a way that the interface becomes steady.

6 Acknowledgements

The author is grateful to Professor G.M.Homsy for numerous valuable suggestions. This work was partially supported by the National Science Foundation under Grant No. CTS-0244676.

References

- [1] Darhuber A.A., Troian S.M., and Reisner W.W., *Phys. Rev. E* **64**, 031603 (2001).
- [2] Garnier N., Grigoriev R.O., and Schatz M.F., *Phys. Rev. Lett.* **91**, 054501 (2003).
- [3] Kabov O.A., *Thermophysics and Aeromechanics* **7**, 513 (2000).
- [4] Gramlich C.M., Kalliadasis S., Homsy G.M., and Messer C., *Phys. Fluids* **14**, 1841 (2002).
- [5] Wu D., and Peterson G.P., *J. Thermophys. and Heat Transfer* **5**, 129 (1991).
- [6] Kondic L., and Bertozzi A.L., *Phys. Fluids* **11**, 3560 (1999).
- [7] Eres M.H., Schwartz L.W., and Roy R.V., *Phys. Fluids* **12**, 1278 (2000).
- [8] Goodwin R., and Homsy G.M., *Phys Fluids A* **3**, 515 (1991).
- [9] Mazouchi A., Gramlich C.M., Homsy G.M., *Phys. Fluids* **16**, 1647 (2004).
- [10] Burelbach J.P., Bankoff S.G., and Davis S.H., *J. Fluid Mech.* **195**, 463 (1988).
- [11] Potash M., and Wayner P.C., *Int. J. Heat and Mass Transfer* **15**, 1851 (1972).
- [12] Moosman S., and Homsy G.M., *J. Colloid Interface Sci.* **73**, 212 (1980).
- [13] DasGupta S., Shoenberg J.A., Kim I.Y., and Wayner P.C., *J. Colloid Interface Sci.* **157**, 332 (1993).

- [14] Morris S.J.S., *J. Fluid Mech.* **432** 1 (2001).
- [15] Lyushnin A.V., Golovin A.A., and Pismen L.M., *Phys. Rev. E* **65**, 021602 (2002).
- [16] Anderson D.M., Davis S.H., *Phys. Fluids* **7**, 248 (1995).
- [17] Miller C.A., and Ruckenstein E., *J. Colloid Interface Sci.* **48**, 368 (1974).
- [18] Hocking L.M., *Phys. Fluids A* **5** 793 (1993).
- [19] Indeikina A, and Chang H.-C., A molecular theory for dynamic contact angles, preprint (1999)
- [20] Wu Q., and Wong H., *J. Fluid Mech.* **506**, 157 (2004).
- [21] Ajaev V.S., and Homsy G.M., *J. Colloid Interface Sci.* **240**, 259 (2001).
- [22] Ajaev V.S., Homsy G.M., and Morris S., *J. Colloid Interface Sci.* **254**, 346 (2002).
- [23] Huppert H.E., *Nature* **300**, 427 (1982).
- [24] Troian S.M., Herbolzheimer E., Safran S.A., Joanny J.F., *Europhys. Lett.* **10**, 25 (1989).
- [25] Golovin A.A., Rubinstein B.Y., and Pismen L.M., *Langmuir* **17**, 3930 (2001).
- [26] Zhornitskaya L., Bertozzi A.L., *SIAM J. Numer. Anal.* **37**, 523 (2000).
- [27] Brown P.N., Byrne C.D., and Hindmarsh A.C., *SIAM J. Sci. Stat. Comput.* **10**, 1038 (1989).

- [28] Spaid M.A., and Homsy G.M., *Phys. Fluids* **8**, 460 (1996).
- [29] Veretennikov I., Indeikina A., and Chang H.-C., *J. Fluid Mech.* **373**, 81 (1998).
- [30] Qu D., Rame E., Garoff S., *Phys. Fluids* **14**, 1154 (2002).
- [31] Gokhale S.J., Plawsky J.L.,Wayner P.C., *J. Colloid Interface Sci.* **259**, 354 (2003).

Figure captions

Figure 1 Sketch of gravity driven viscous flow of a volatile liquid on an inclined heated surface (a) and the scaled temperature profile along the solid substrate (b).

Figure 2 Interface shape (a) and the linear-log plot of the vicinity of the transition region (b) for the gravity-driven viscous flow in the limit of weak evaporation ($\bar{E} = 10^{-4}$) for $K = 0.2, \delta = 10^{-3}, \varepsilon = 10^{-6}, T_H = 0.5, M = 0, \beta = 1, \alpha = \pi/4, L = 20$.

Figure 3 Velocity of the point of maximum of the interface at $\bar{t} = 100$ as a function of the scaled evaporation number for $K = 0.2, \delta = 10^{-3}, \varepsilon = 10^{-6}, M = 0, \beta = 1, \alpha = \pi/4, L = 30$.

Figure 4 Height of the capillary ridge as a function of scaled time for different parameter values: (a) $\bar{E} = 0.001$ (solid line) and $\bar{E} = 0.01$ (dashed line) with $T_H = 0.5$; (b) $T_H = 1.0$ (solid line) and $T_H = 2.0$ (dashed line) with $\bar{E} = 0.001$. Results for the weak evaporation limit are also shown (dot-dashed lines) for comparison.

Figure 5 Position (a) and the value (b) of the maximum of the interfacial height as functions of \bar{t} for $K = 0.2, \delta = 10^{-3}, \varepsilon = 10^{-6}, \bar{E} = 0.01, \beta = 0, \alpha = \pi/4$ and different values of the modified Marangoni number: $M = 1$ (solid line) and $M = 0$ (dashed line).

Figure 6 Position of the maximum of the interfacial height as a function of scaled time for $K = 0.2, \delta = 10^{-3}, \varepsilon = 10^{-6}, \bar{T}_H = 0.5, M = 0, \beta = 0, \alpha = \pi/4$, and different values of the scaled evaporation number: $\bar{E} = 0.04$ (solid line), $\bar{E} = 0.02$ (dashed line), and $\bar{E} = 0.01$ (dot-dashed line).

Figure 7 Apparent contact angle as a function of scaled heater temperature (a) and the degree of inclination measured by $\sin \alpha$ at $\bar{T}_H = 2$ (b) for $K = 0.2, \delta = 10^{-3}, \varepsilon = 10^{-6}, \bar{E} = 10^{-3}, M = 0, \beta = 1$.

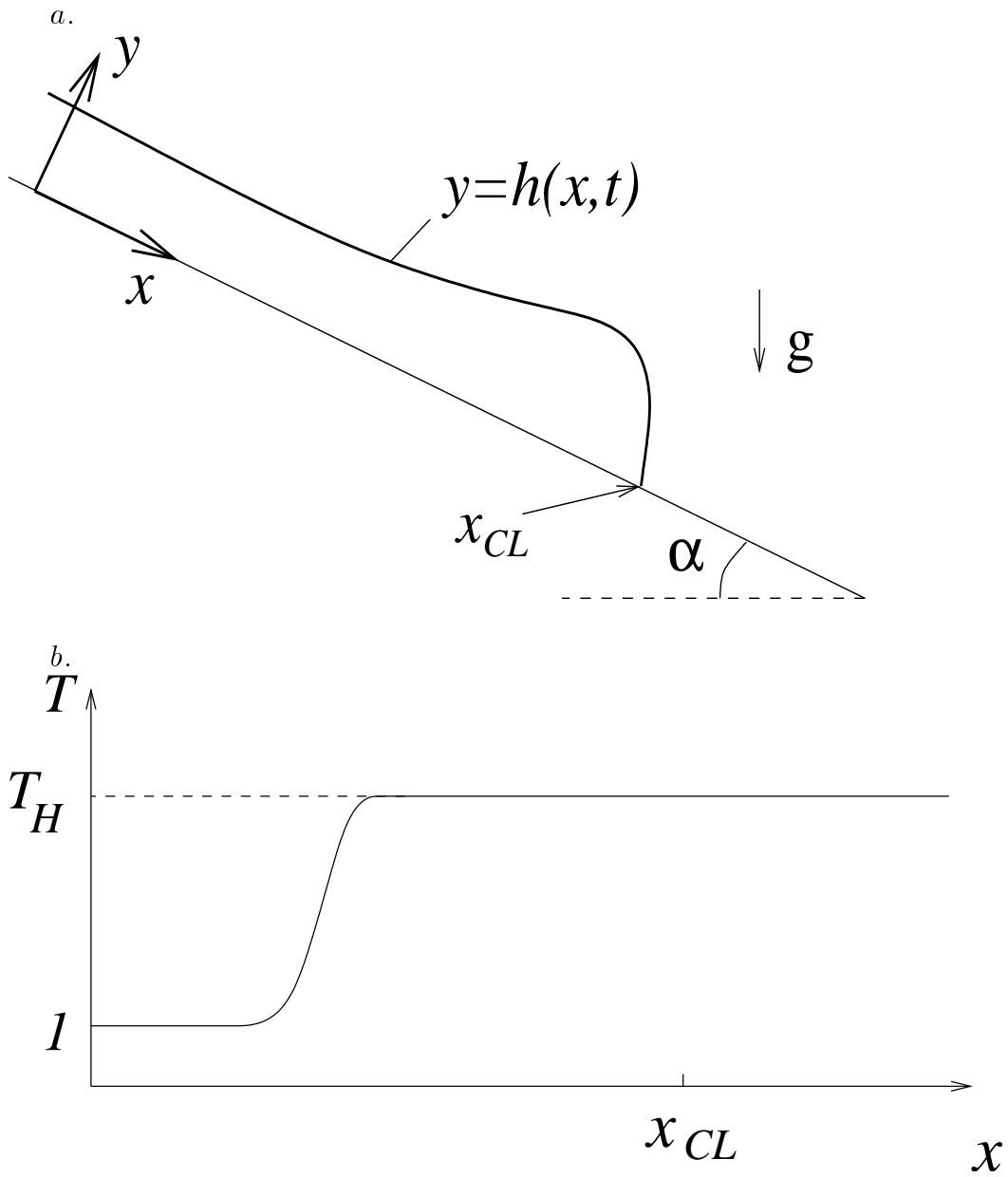


Figure 1 Sketch of gravity driven viscous flow of a volatile liquid on an inclined heated surface (a) and the scaled temperature profile along the solid substrate (b).

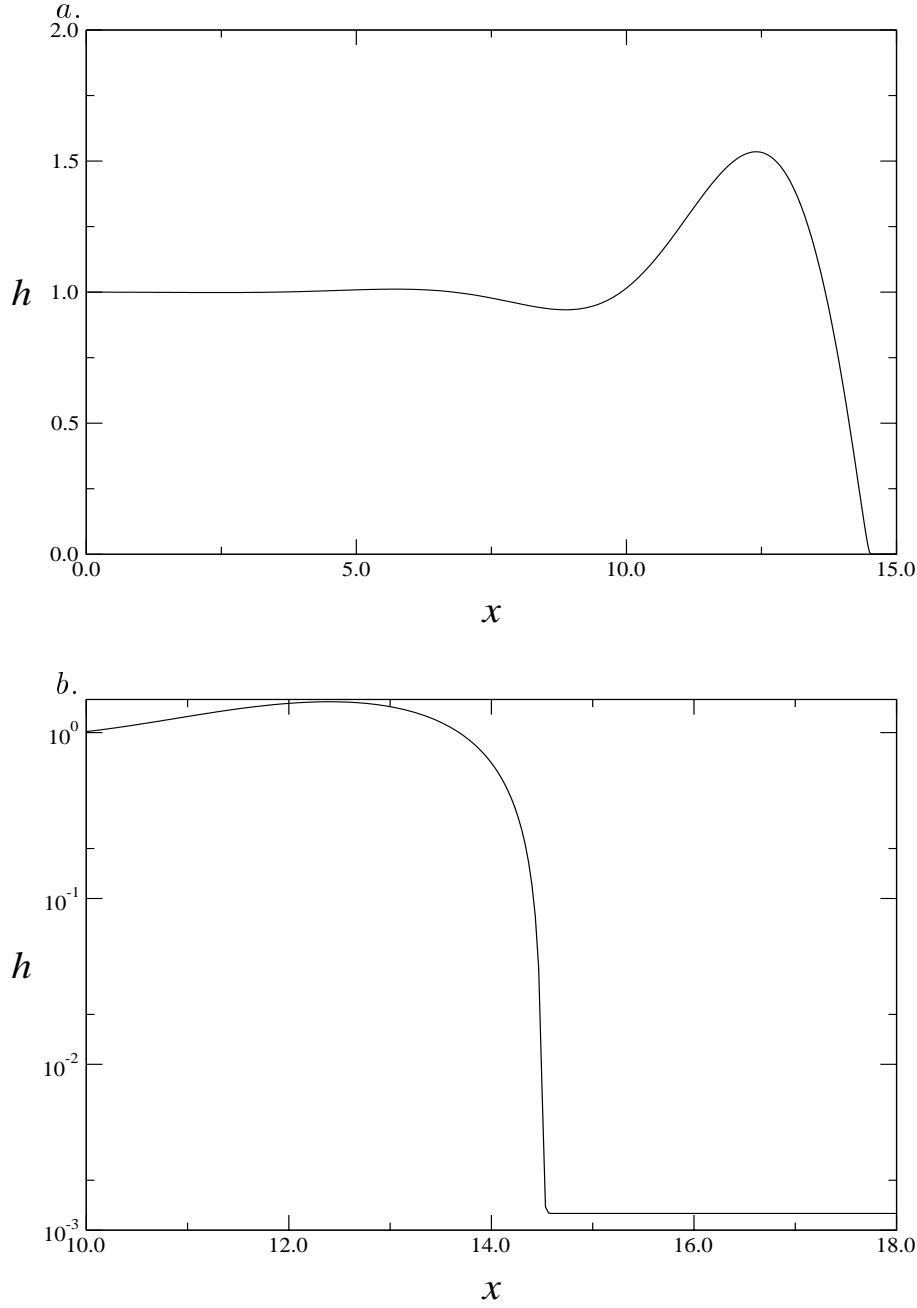


Figure 2 Interface shape (a) and the linear-log plot of the vicinity of the transition region (b) for the gravity-driven viscous flow in the limit of weak evaporation ($\bar{E} = 10^{-4}$) for $K = 0.2, \delta = 10^{-3}, \varepsilon = 10^{-6}, T_H = 0.5, M = 0, \beta = 1, \alpha = \pi/4, L = 20$.

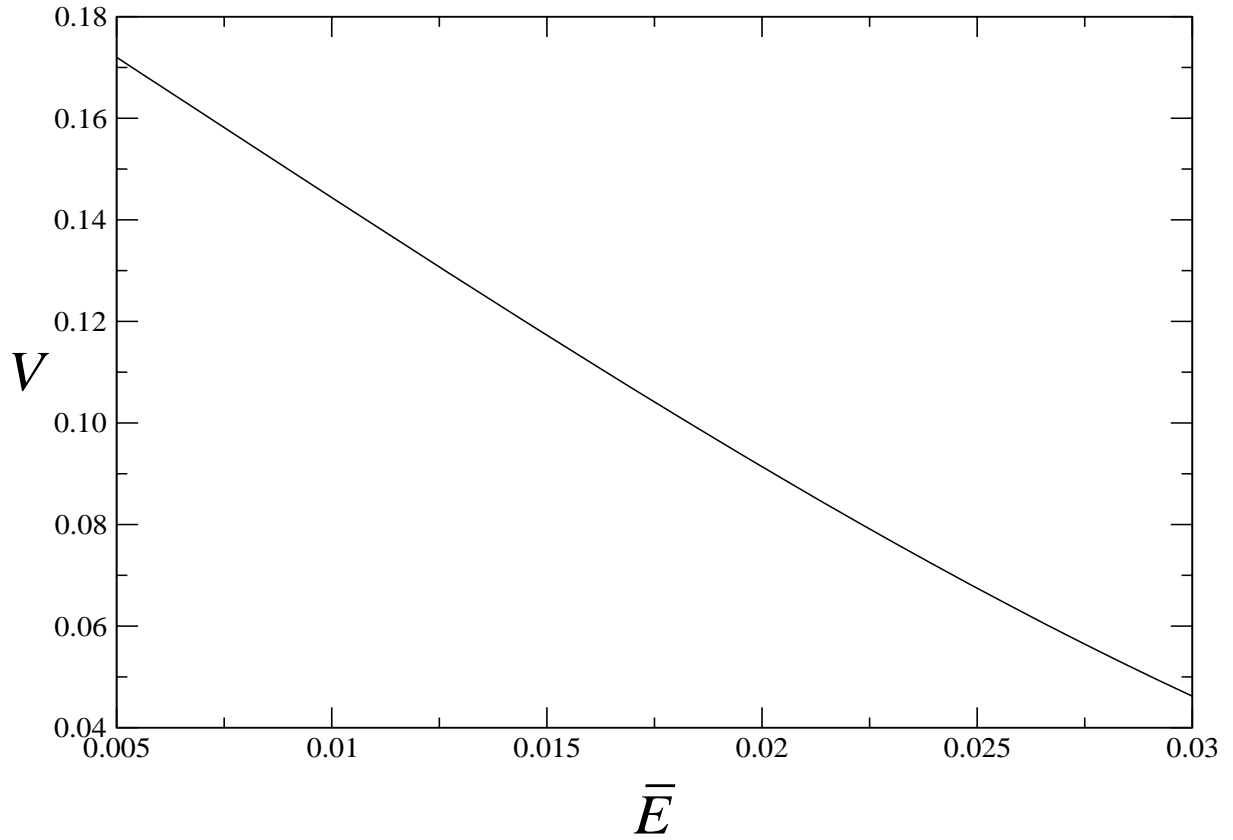


Figure 3 Velocity of the point of maximum of the interface at $\bar{t} = 100$ as a function of the scaled evaporation number for $K = 0.2, \delta = 10^{-3}, \varepsilon = 10^{-6}, M = 0, \beta = 1, \alpha = \pi/4, L = 30$.

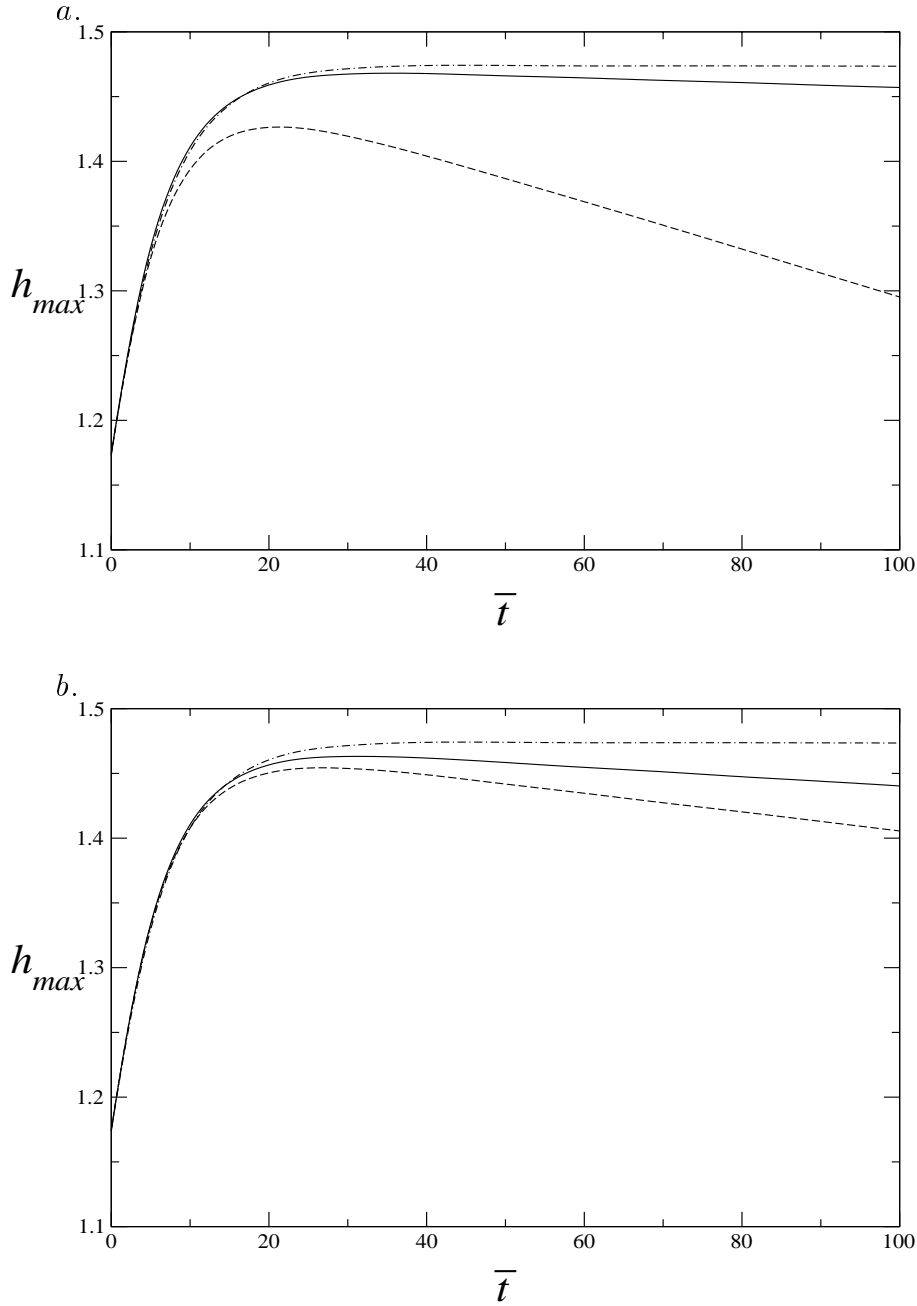


Figure 4 Height of the capillary ridge as a function of scaled time for different parameter values: (a) $\bar{E} = 0.001$ (solid line) and $\bar{E} = 0.01$ (dashed line) with $\bar{T}_H = 0.5$; (b) $\bar{T}_H = 1.0$ (solid line) and $\bar{T}_H = 2.0$ (dashed line) with $\bar{E} = 0.001$. Results for the weak evaporation limit are also shown (dot-dashed lines).

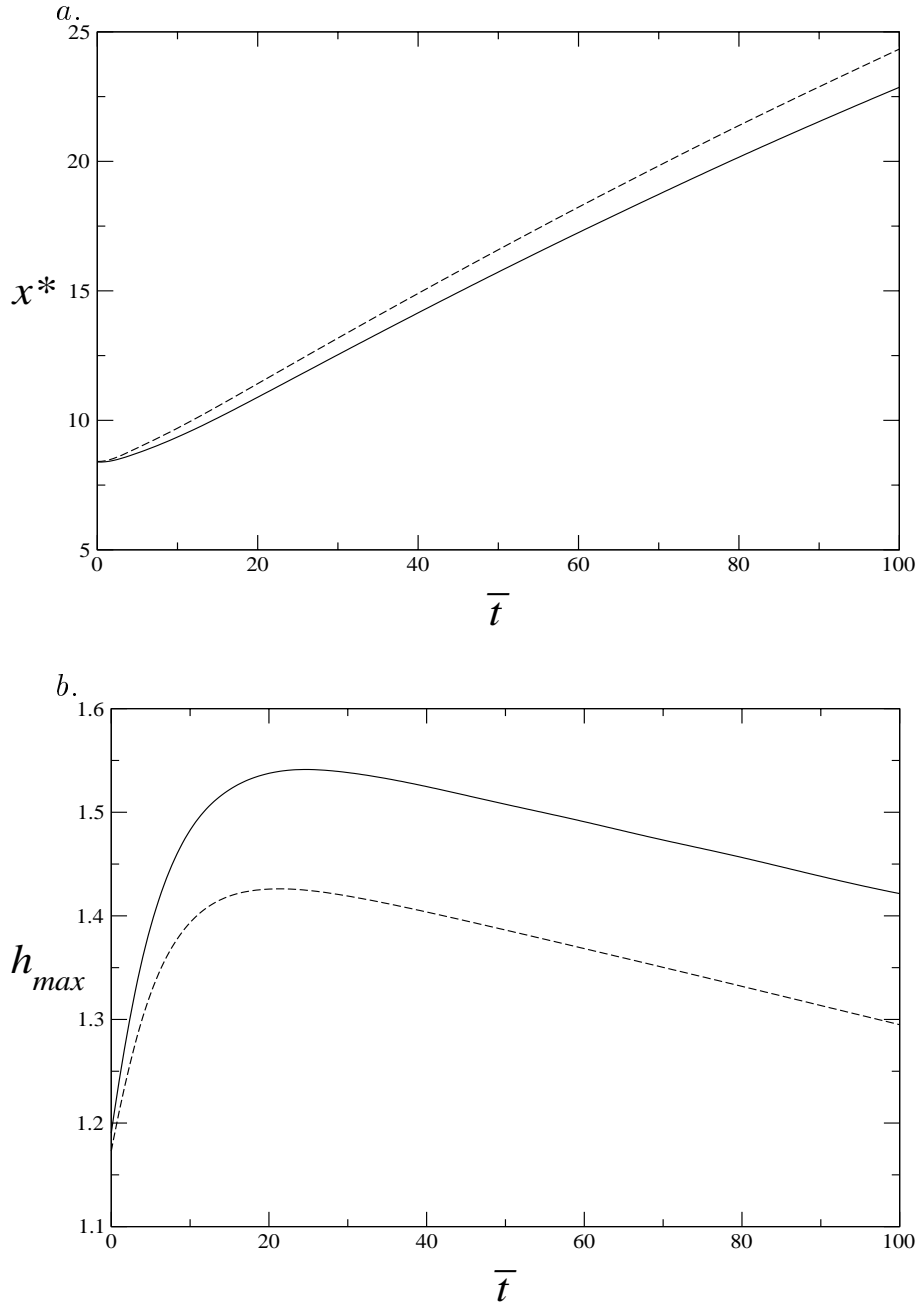


Figure 5 Position (a) and the value (b) of the maximum of the interfacial height as functions of \bar{t} for $K = 0.2, \delta = 10^{-3}, \varepsilon = 10^{-6}, \bar{E} = 0.01, \beta = 0, \alpha = \pi/4$ and different values of the modified Marangoni number: $M = 1$ (solid lines) and $M = 0$ (dashed lines).

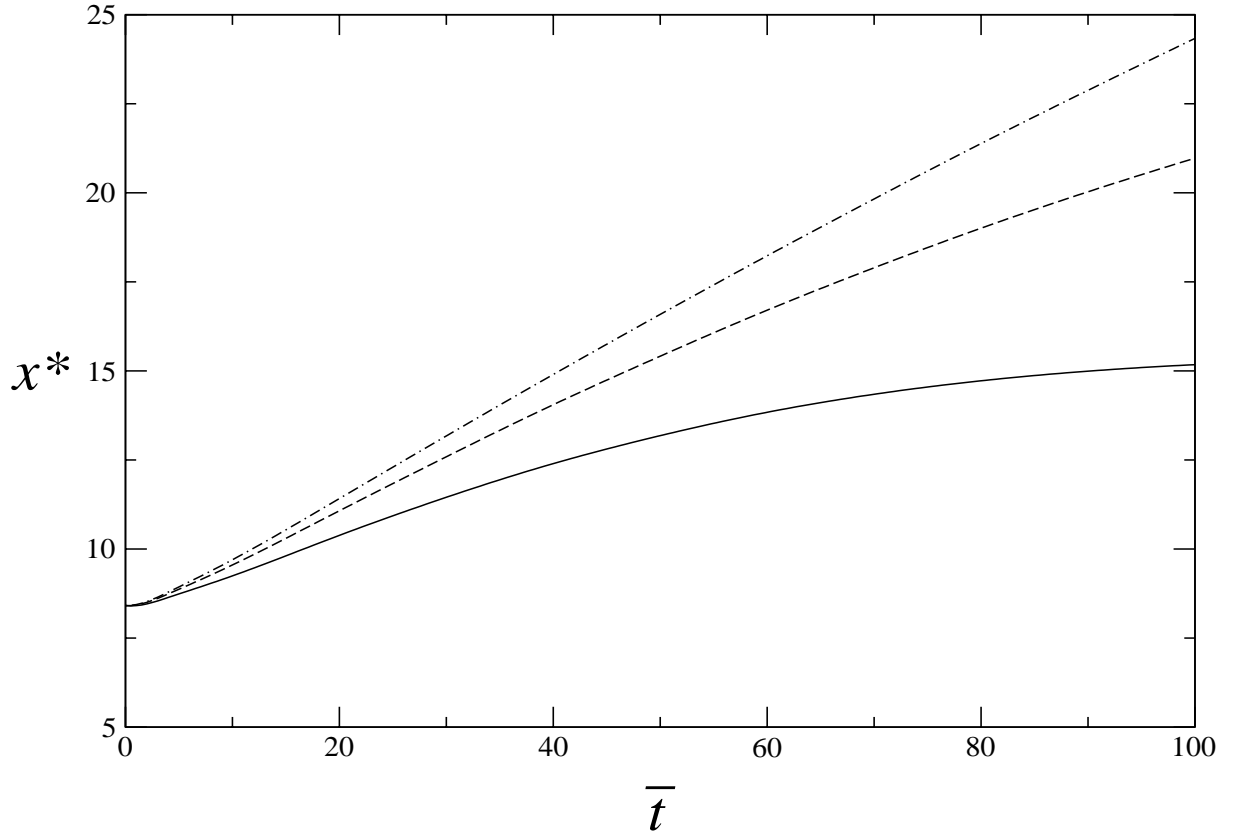


Figure 6 Position of the maximum of the interfacial height as a function of scaled time for $K = 0.2, \delta = 10^{-3}, \varepsilon = 10^{-6}, \bar{T}_H = 0.5, M = 0, \beta = 0, \alpha = \pi/4$, and different values of the scaled evaporation number: $\bar{E} = 0.04$ (solid line), $\bar{E} = 0.02$ (dashed line), and $\bar{E} = 0.01$ (dot-dashed line).

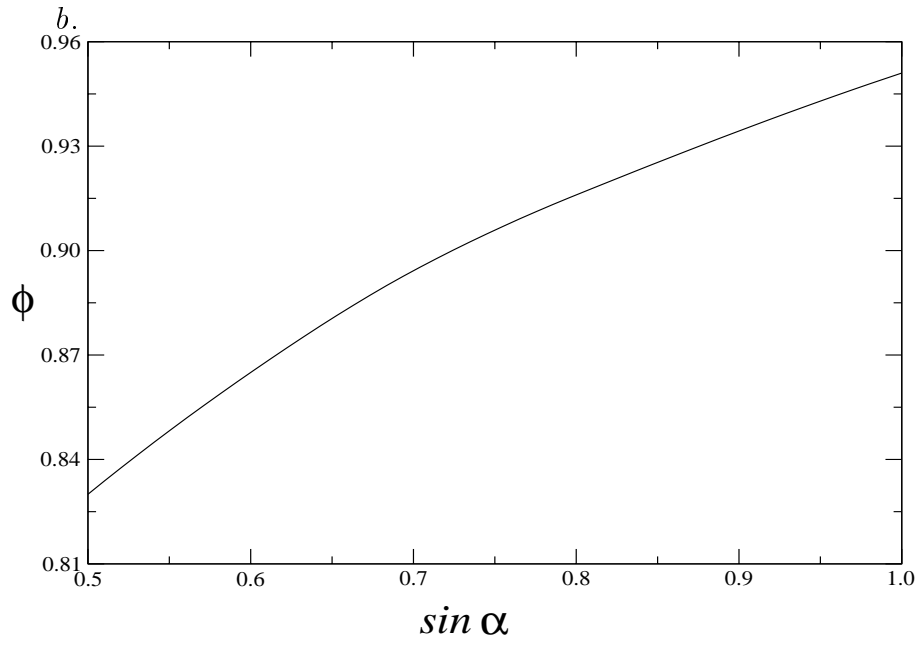
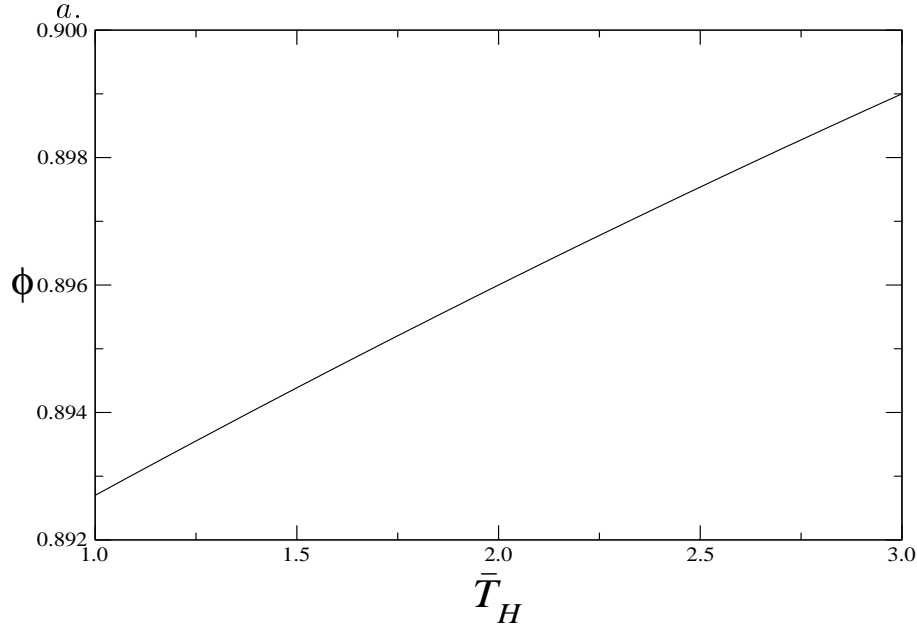


Figure 7 Apparent contact angle as a function of scaled heater temperature (a) and the degree of inclination measured by $\sin \alpha$ at $\bar{T}_H = 2$ (b) for $K = 0.2, \delta = 10^{-3}, \varepsilon = 10^{-6}, \bar{E} = 10^{-3}, M = 0, \beta = 1$.